Data-driven approach to parameterize SCAN + U for an accurate description of 3d transition metal oxide thermochemistry

Nongnuch Artrith [1,*] José Antonio Garrido Torres,[1] Alexander Urban [1] and Mark S. Hybertsen [2,†]
[1]*Department of Chemical Engineering, Columbia University, New York, New York 10027, USA*
[2]*Center for Functional Nanomaterials, Brookhaven National Laboratory, Upton, New York 11973, USA*

(Received 12 September 2021; revised 3 February 2022; accepted 7 March 2022; published 23 March 2022)

Semilocal density-functional theory (DFT) methods exhibit significant errors for the phase diagrams of transition-metal oxides that are caused by an incorrect description of molecular oxygen and the large self-interaction error in materials with strongly localized electronic orbitals. Empirical and semiempirical corrections based on the DFT + U method can reduce these errors, but the parameterization and validation of the correction terms remains an on-going challenge. We develop a systematic methodology to determine the parameters and to statistically assess the results by considering interlinked thermochemical data across a set of transition metal compounds. We consider three interconnected levels of correction terms: (1) a constant oxygen binding correction, (2) Hubbard-U correction, and (3) DFT/DFT + U compatibility correction. The parameterization is expressed as a unified optimization problem. We demonstrate this approach for 3d transition metal oxides, considering a target set of binary and ternary oxides. With a total of 37 measured formation enthalpies taken from the literature, the dataset is augmented by the reaction energies of 1710 unique reactions that were derived from the formation energies by systematic enumeration. To ensure a balanced dataset across the available data, the reactions were grouped by their similarity using clustering and suitably weighted. The parameterization is validated using leave-one-out cross validation (CV), a standard technique for the validation of statistical models. We apply the methodology to the strongly constrained and appropriately normed (SCAN) density functional. Based on the CV score, the error of binary (ternary) oxide formation energies is reduced by 40% (75%) to 0.10 (0.03) eV/atom. A simplified correction scheme that does not involve SCAN/SCAN + U compatibility terms still achieves an error reduction of 30% (25%). The method and tools demonstrated here can be applied to other classes of materials or to parameterize the corrections to optimize DFT + U performance for other target physical properties.

DOI: 10.1103/PhysRevMaterials.6.035003

I. INTRODUCTION

Density-functional theory (DFT) [1,2] has become a standard tool for computational materials design [3–6]. However, conventional (semi-)local DFT methods based on the generalized gradient approximation (GGA) [7] exhibit a self-interaction error (SIE) that can lead to an over-delocalization of electrons, resulting in an incorrect description of many TM oxides with strongly localized d electrons [8–10]. In addition, bonds with high bond order are found to be relatively overbound when computed with local and semilocal exchange-correlation functionals, such as the widely used GGA functional by Perdew, Burke, and Ernzerhof (PBE) [11]. Specifically, the strength of the O–O bond in the dioxygen molecule is too strongly bound (by ∼3.4 eV for the PBE functional) [12], which introduces an additional systematic error in the formation energies of oxides [13,14]. For applications involving transition metal (TM) oxides, empirical corrections for both the SIE and the overbinding of oxygen are therefore often introduced [14–19], the values of which have to be carefully fitted and validated.

Accounting for strong, local Coulomb interactions between electrons in the TM d states approximately through the DFT + U method has been particularly successful for reducing the SIE in TM oxides without significantly increasing the computational cost [15,16]. DFT + U introduces TM-specific Hubbard U parameters representing the local, screened Coulomb interaction. They can be either obtained from linear-response theory [20–22] or empirically by fitting reference properties such as reaction energies [14,17,18,23–25] or band gaps from experiment or more accurate electronic structure calculations [16]. In combination with an empirical energy correction for the overbinding of the O-O bond [14] and a compatibility correction that accounts for the mixing of PBE and PBE + U calculations [24], PBE/PBE + U often reproduces TM oxide formation energies with sufficient accuracy so that derived phase diagrams are in agreement with experiment [25,26]. A related, alternative to separate corrections for oxygen overbinding and DFT/DFT + U compatibility is the fitting of empirical reference energies for all chemical species, which can also yield improved formation energies [17,18].

One challenge in the parameterization of DFT + U methods is the dependence of the optimal Hubbard U parameter

*Present Address: Materials Chemistry and Catalysis, Debye Institute for Nanomaterials Science, Utrecht University, 3584 CG Utrecht, The Netherlands, n.artrith@uu.nl
†mhyberts@bnl.gov

on the oxidation state of the metal center [27,28]. Energies obtained from DFT + U calculations with different U values lack a common reference and are therefore not generally compatible. In practice, energies associated with oxidation or reduction reactions must be calculated with average U values that are a compromise for all involved valence states [28]. DFT + U is a static correction to DFT and does not capture, for example, frequency-dependent screening by delocalized electrons [21], which would call for more complex theories, such as DFT+DMFT [29,30]. Furthermore, the convergence of DFT + U calculations to the self-consistent electronic ground state becomes more challenging with increasing U values [26,31].

While some of the challenges of DFT + U are intrinsic to the approach, the choice of exchange-correlation functional also plays an important role for the accuracy that DFT + U calculations can achieve. For example, PBE + U predicts an incorrect hybridization of TM and O states for oxides in which the TM d states are close in energy to the O $2p$ states [27]. This electronic-structure error cannot be removed with an empirical energy correction and requires an additional electronic-structure correction, such as an additional Hubbard-U term for the O $2p$ states [32–34]. Intuitively, a functional that predicts oxide formation energies more accurately than PBE should also provide a more robust starting point for the modeling of transition-metal oxides with the addition of empirical corrections.

The recently proposed strongly constrained and appropriately normed (SCAN) meta-GGA functional has shown promise for the prediction of oxide phase diagrams with greater accuracy and less empiricism than GGA functionals [35–44]. Compared to PBE, SCAN exhibits a significantly reduced O_2 overbinding error, ∼0.3 eV [35]. Prior studies concluded that SCAN does not entirely remove the SIE, and a Hubbard-U correction is still required for many 3d TM species, albeit with the magnitude of the U values being smaller than required for PBE in applications considered to date [37–41,43–47]. The performance of SCAN/SCAN + U for the prediction of TM oxide *formation energies* has, to our knowledge, not yet been investigated.

In the present work, we determine the parameters for the three levels of corrections needed to facilitate quantitative formation-energy calculations with SCAN/SCAN + U: (i) the O–O binding energy correction, (ii) the Hubbard-U electronic-structure correction of the TM d states, and (iii) the SCAN/SCAN + U compatibility correction. To accomplish this parameterization in a systematic and unbiased fashion, we propose a methodology for the automated fit of Hubbard-U values and DFT/DFT + U compatibility corrections to experimental formation energies from the literature and derived reaction energies. By considering a large, interconnected set of compounds simultaneously, we are able to apply quantitative metrics that give a statistical outlook for the derived parameters. We note that a partially automated fitting of O_2 corrections, U values and PBE/PBE + U compatibility corrections have recently been reported by Mutter *et al.* for a set of iron oxide compounds [48]. Here, we formalize such U parameterization as a regularized optimization problem and apply it to SCAN + U. In our approach, an exhaustive set of oxide reactions is derived from the formation energies, ensuring an unbiased representation of the relative energies of all oxides in the reference data set and providing statistical error estimates of the U values.

Specifically, we demonstrate and apply the framework to determine an optimal parameterization of SCAN + U for the prediction of the formation energies of binary and ternary oxides of the 3d TM species Ti, V, Cr, Mn, Fe, Co, Ni, and Cu, as well as energies of reactions involving the oxide species. We report benchmarks of reaction and formation energies that were not included in the optimization procedure and assess the impact of the $+U$ correction on the prediction of oxide phase diagrams. The reference data set contains 37 formation energies and 1710 oxide reaction energies that were derived from the formation energies.

Our methodology optimizes U values for a family of transition metal oxide reactions and formation reactions incorporating robust statistical methods that remove arbitrariness from the determination of empirical corrections in DFT + U approaches. It provides error estimates both for the parameters and for the prediction of reaction energies, including the impact of transferability of the parameters. Key elements of the approach include regularized least-squares optimization, cross validation, and grouping of similar oxide and formation reactions using principal component analysis and k-means clustering to remove biases from the reference data set. Leveraging this framework and the new SCAN functional yields a SCAN/SCAN + U parameterization for accurate calculations of 3d TM metal and oxide reactions.

In Sec. II, we describe the theoretical background and the essential features of our framework. The main results are presented in Sec. III and further discussion appears in Sec. IV. We summarize and conclude the paper in Sec. V.

II. METHODS

A. Terminology and definitions

The formation of a binary TM oxide A_xO_y (A = TM species) from the elemental metal and oxygen gas is described by the general *formation reaction*

$$\left(xA + \frac{y}{2}\, O_2 \rightarrow A_x\, O_y \right). \tag{1}$$

The enthalpy of formation $\Delta_f H(A_xO_y)$ is defined as the heat of reaction of the formation reaction, i.e., the enthalpy difference between the products and reactants in Eq. (1). At zero Kelvin, ignoring corrections due to zero-point fluctuations, the enthalpy of formation can be approximated as the difference of the DFT energies (E_{DFT}) of the reactants and products

$$\begin{aligned}\Delta_f H(A_xO_y) &\approx \Delta_f H_{\mathrm{DFT}}(A_xO_y) \\ &= E_{\mathrm{DFT}}(A_xO_y) - x\, E_{\mathrm{DFT}}(A) - \frac{y}{2} E_{\mathrm{DFT}}(O_2).\end{aligned} \tag{2}$$

The definition for ternary oxides is equivalent, and the enthalpy of formation of a ternary oxide $A_xB_yO_z$ is given by

$$\begin{aligned}\Delta_f H_{\mathrm{DFT}}(A_xB_yO_z) = E_{\mathrm{DFT}}(A_xB_yO_z) - x\, E_{\mathrm{DFT}}(A) \\ - y\, E_{\mathrm{DFT}}(B) - \frac{z}{2} E_{\mathrm{DFT}}(O_2).\end{aligned} \tag{3}$$

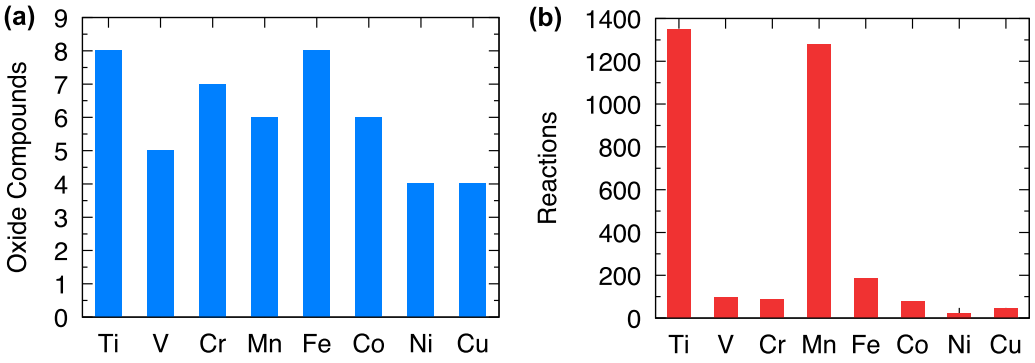

FIG. 1. Representation of different transition-metal species in our data set. (a) Number of oxide compounds with formation enthalpies in our reference data set. (b) Number of derived oxide and O_2 reactions. See Tables S1 and S2 for a complete list.

In the following, we refer to zero-Kelvin formation enthalpies simply as *formation energies*.

The heat of reaction $\Delta_r H$ of a general reaction can be expressed in terms of formation energy differences of reaction products P and reactants R

$$\Delta E = \Delta_r H = \sum_{P}^{\text{Products}} \Delta_f H(P) - \sum_{R}^{\text{Reactants}} \Delta_f H(R), \qquad (4)$$

which we refer to as *reaction energy* ΔE in the following.

In addition to formation reactions, we also consider the reaction energies of solid-state reactions. Here, we distinguish between pure *oxide reactions not involving elemental oxygen* (O_2) and *oxide reactions involving* O_2. Oxide reactions not involving O_2 are reactions in which all reactants and products are oxides, such as

$$A_x O_{z_1} + B_y O_{z_2} \rightarrow A_x B_y O_{z_1+z_2}. \qquad (5)$$

Such oxide reactions do not typically involve the change of oxidation states, and we expect therefore that a single U value can be found that is simultaneously (close to) optimal for the reactants and products. In contrast, in oxide reactions that involve elemental oxygen as either reactant or product at least one TM species has to be subject to a change of oxidation state, as elemental oxygen has an oxidation state of zero whereas the formal oxidation state of oxygen in oxides is -2

$$A_x O_y + \tfrac{1}{2} O_2 \rightarrow A_x O_{y+1} \quad \text{with} \quad y > 0. \qquad (6)$$

Calculating the reaction energies of such reactions might require an average U value that is neither optimal for the reactants nor for the products, since the optimal Hubbard U parameter can vary with the oxidation state [20,27].

B. Reference data

Our database contains the experimental formation enthalpies of 24 binary oxides ($A_x O_y$) and 13 ternary oxides ($A_x B_y O_z$) of $3d$ TMs from the literature [24,49–53]. In the analysis of the O–O binding energy correction, we also consider a sample of other oxides (Al_2O_3, CaO, Li_2O, MgO, Na_2O, Sc_2O_3, SiO_2, SnO_2, ZnO, ZrO_2). Our calculations correspond to 0 K and 0 atm, but we chose reference enthalpies at standard conditions (298 K and 1 atm) for which more data is available. The enthalpy difference $\Delta_f H^{0\text{K}} - \Delta_f H^{298\text{K}}$ has previously been estimated to be typically less than 0.03 eV/atom [17,24], so that this error is not significant. See Supplemental Material Tables S1 and S3 [54] for a complete list of compounds and the original references. We did not consider a Hubbard-U correction for Sc_2O_3 and ZnO, since Sc^{3+} and Zn^{2+} have an empty and filled $3d$ band, respectively. In such cases, Hubbard-U corrections are usually not needed. As an important validation of this assumption, our computations with the uncorrected SCAN functional accurately predict the formation enthalpies of ZnO and Sc_2O_3 with errors of $0.045\,\text{eV}/O_2$ and $0.026\,\text{eV}/O_2$, respectively (see also Table S3). The frequency of occurrence of the other $3d$ TMs in our reference data set is visualized in Fig. 1(a).

From the data set of $24 + 13 = 37$ experimental formation enthalpies, the energies of oxide reactions (with and without O_2 as reactant) can be derived according to Eq. (4). We used the python materials genomics (PYMATGEN) [55] package for enumerating all unique oxide reactions involving the 37 oxide compounds, yielding a derived database of 1,710 unique reaction energies (Table S2). Note that the frequency of occurrence of the different TM species in the derived reaction database varies, as seen in Fig. 1(b). Ni is represented by the smallest number of reactions (seven). On the other hand, Ti, Mn, and Fe form oxides with three different oxidation states and measured formation energies are available for more compounds. The derived reaction data set therefore contains a large number of reactions involving these three species.

C. Grouping of similar reactions

For some species, many reactions have similar reactants, potentially leading to an overrepresentation in the reference data set. To systematically balance the data set, we propose a metric for reaction similarity, use it to group similar reactions, and thus determine a shared weight for the reactions in the optimization. Specifically, each chemical reaction was represented as a vector with 57 components, each of which represents the coefficient of one of the compounds in our library (37 oxides and their base elements). We employ the convention that reactant coefficients are negative and product coefficients are positive, so that the reaction energy of Eq. (4) can be expressed as the scalar product $\Delta E = \vec{r}\,\vec{e}_U$, where $\vec{r}$ is the vector with reaction coefficients and $\vec{e}_U$ is a vector with the

computed compound energies for a specific set of U values. In this representation, a grouping of similar reactions was achieved in two steps by (1) reducing the dimension of the reaction representation via principal component analysis (PCA) [56] and (2) performing a cluster analysis using k-means clustering [57]. A reference to the PYTHON code implementing the reaction grouping methodology (using *scikit-learn* [58]) is given in the data availability section below. Reactions that are assigned to the same cluster are considered similar in our optimization procedure and enter with a shared weight. This means, all N_i reactions within a cluster i enter the optimization procedure with a weight of $1/N_i$.

D. Empirical corrections of DFT errors: Parameter determination

The parameterization of the three empirical correction terms in the DFT + U methodology described in the introduction are formulated as formal optimization problems.

O–O overbinding affects the prediction of reaction energies that involve elemental oxygen, i.e., formation energies and O_2 reaction energies. We employ the technique by Wang *et al.* [14], determining a constant correction to the energy of the O_2 molecule by comparison of predicted formation energies from DFT calculations and the corresponding reference energies from tabulated experiments. Expressing this as an optimization problem, we introduce the *objective function* (or *loss function*)

$$L_{O_2} = \sum_i \left(\left[E_{\mathrm{DFT}}(\sigma_i) + \frac{n_O(\sigma_i)}{2} \varepsilon_{O_2} \right] - \Delta_f H(\sigma_i) \right)^2, \quad (7)$$

where σ_i is an oxide composition and $n_O(\sigma_i)$ is the number of oxygen atoms in σ_i. The optimal O_2 correction energy $\varepsilon_{O_2}^{\mathrm{corr}}$ is then determined by minimizing the objective function

$$\varepsilon_{O_2}^{\mathrm{corr}} = \arg\min_{\varepsilon_{O_2}} L_{O_2}. \quad (8)$$

For the correction of the SIE, we employ a rotationally invariant Hubbard-U term [16] for the TM d bands, adjusting the U values such that experimental reaction energies are reproduced as well as possible. The objective function for the U-value optimization is therefore

$$L_U = \sum_i^N (\Delta E_{\mathrm{DFT}+U}(\rho_i,\ \{U\}_{\mathrm{TM}}) - \Delta E(\rho_i))^2, \quad (9)$$

where ρ_i is a reaction, N is the total number of reactions in the reference data set, $\Delta E_{\mathrm{DFT}+U}(\rho_i,\ \{U\}_{\mathrm{TM}})$ is the reaction energy of ρ_i predicted by DFT + U calculations using the set of U values $\{U\}_{\mathrm{TM}}$, and $\Delta E(\rho_i)$ is the experimental reaction energy as defined in Eq. (4). The optimal U values are those that minimize the objective function L_U, and the *root mean squared error*, $\mathrm{RMSE} = \sqrt{L_U/N}$, provides a statistical estimate of the standard deviation of predicted reaction energies.

We employ the Hubbard-U correction only for the TM d bands in TM oxides and not for the elemental metals, since electrons in metals are delocalized and are already well described by uncorrected local and semilocal DFT [59]. This means, the reaction energies of oxide reactions can be calculated consistently with DFT + U, since TM species only occur in oxide form. However, formation reactions involve both elemental (metallic) TM species, which are best described by uncorrected DFT, and their oxides, which require DFT + U [24].

To ensure that the energies from DFT and DFT + U calculations are compatible, we explore two different strategies: (1) We determine the optimal set of U values by minimizing L_U for a reference data set containing oxide reactions, both those involving and those not involving O_2, and formation reactions. In this approach, DFT/DFT + U compatibility is implicit to the objective function, and the optimal U values will allow calculation of energy differences by combining DFT and DFT + U calculations as needed for formation energies. (2) We employ an additional DFT/DFT + U compatibility correction following Jain *et al.* [24] for the calculation of formation energies.

The DFT/DFT + U correction by Jain *et al.* [24] introduces another set of TM-species dependent correction parameters $\{\mu\}_{\mathrm{TM}}$ that are applied to all energies from DFT + U calculations, yielding *renormalized* DFT + U energies

$$E_{\mathrm{DFT}+U}^{\mathrm{renorm}}(\sigma) = E_{\mathrm{DFT}+U}(\sigma) - \sum_M n_M(\sigma)\mu_M \quad (10)$$

where the sum runs over all considered TM species M and $n_M(\sigma)$ is the number of atoms of species M in composition σ. With this compatibility correction, formation energies can be calculated by combining DFT calculations of the metals and renormalized DFT + U calculations of the oxides, e.g., for binary oxides

$$\begin{aligned} &\Delta_f H_{\mathrm{DFT/DFT}+U}(M_xO_y) \\ &\quad = E_{\mathrm{DFT}+U}^{\mathrm{renorm}}(M_xO_y) - xE_{\mathrm{DFT}}(M) - \frac{y}{2}E_{\mathrm{DFT}}(O_2) \\ &\quad = E_{\mathrm{DFT}+U}(M_xO_y) - x\,\mu_M - x\,E_{\mathrm{DFT}}(M) - \frac{y}{2}E_{\mathrm{DFT}}(O_2). \end{aligned} \quad (11)$$

An objective function for the determination of the parameters $\{\mu\}_{\mathrm{TM}}$ can be formulated as

$$L_\mu = \sum_i (\Delta_f H_{\mathrm{DFT/DFT}+U}(\sigma_i, \{U\}_{\mathrm{TM}}, \{\mu\}_{\mathrm{TM}}) - \Delta_f H(\sigma_i))^2, \quad (12)$$

where the sum runs over oxide compositions σ_i. Note that the value of the DFT/DFT + U compatibility correction parameters $\{\mu\}_{\mathrm{TM}}$ depends on the choice of the U values. Hence, the optimization of U parameters with the objective function L_U of Eq. (9) and the calculation of the compatibility correction parameters has to be done simultaneously.

In the scope of the reactions in our dataset, the Jain correction specifically affects the formation energies where the elemental TM crystals are a reactant. It does not affect the oxide reactions, independent of whether O_2 is a reactant.

The parameters were determined as follows:

First, the O_2 correction energy $\varepsilon_{O_2}^{\mathrm{corr}}$ for SCAN was obtained as described in Eq. (8), i.e., by minimizing the objective function L_{O_2}. The O_2 correction is purely a correction of the energy of the O_2 molecule as predicted by DFT, and it is therefore independent of the choice of U values.

Next, U values were determined via iterative least-squares optimization, as schematically shown in the flowchart of Fig. S1. The optimization of U values was performed by minimizing the objective function L_U of Eq. (9) with the two strategies described in the previous sections, i.e., (1) by fitting the entire database including oxide reaction energies and formation energies, and (2) by fitting only oxide reaction energies and introducing an additional SCAN/SCAN + U compatibility correction following Jain *et al.* (*Jain correction*) [24].

To remove unnecessary flexibility from the regression, we introduce another condition: If two sets of U values yield overall equivalent accuracy, U values with smaller magnitude should be preferred. To bias the optimization to smaller U values, we make use of L2 regularization [60] and introduce an additional term into the objective function L_U of Eq. (9) that scales with the norm of the U values

$$L_U^{\text{reg}} = L_U + \lambda \sum_M |U_M|^2. \tag{13}$$

Determination of λ is discussed in Sec. III B.

E. Validation and error quantification

While the goodness-of-fit metric provides a criterion for the overall accuracy of each version of the DFT + U scheme across the data set, leave-one-out cross-validation (LOOCV) is a standard error quantification technique for statistical models that provides a much more robust validation criterion [61,62]. Here, we estimate the accuracy of our SCAN + U parameterization using LOOCV. In practice, this means that the optimization procedure of Fig. S1 is repeated 37 times. Each time, one of the compounds σ_i with $1 \leqslant i \leqslant 37$ selected from the set of 24 binary and 13 ternary oxides is removed from the reference data set along with all reactions in which it occurs. For the remaining 36 compounds and the associated derived reactions, the full analysis procedure is carried out, including grouping the reactions via PCA and k-means clustering followed by the parameterization optimization. The resulting SCAN + U parameters are then used to evaluate the prediction error for the formation energy of compound σ_i and the reaction energies of all reactions involving compound σ_i. Hence, all predicted SCAN + U formation and reaction energies reported in the following are true predictions of reaction energies outside the reference data set entering the least-squares optimization.

Another benefit of the LOOCV method is that it provides a sensitivity analysis for the obtained Hubbard-U and Jain compatibility correction values. Leaving out compound σ_i from the optimization affects the optimal U values for the TM species in σ_i. Thus, from LOOCV we obtain a distribution of U values for each TM species. The spread of values indicates how sensitive the U value is with respect to the chosen reference data set.

F. Computational details: Density-functional theory calculations

All DFT calculations were performed within the projector-augmented wave (PAW) formalism [63] as implemented in the Vienna *Ab Initio* Simulation Package (VASP) [64–67]. VASP input files were generated using the Python Materials Genomics (pymatgen) toolkit [55]. All calculations employed the SCAN meta-GGA exchange-correlation functional [35] and the rVV10 dispersion correction [36,68]. A plane wave energy cutoff of 520 eV was employed for the representation of the wave functions, and automatically generated regular Γ-centered k-point meshes with a length parameter of $R_k = 25$ were employed for the integration of the Brillouin zone. The convergence threshold for self-consistent field calculations was 10^{-5} eV, and geometry optimizations minimized the atomic forces to less than 0.1 eVÅ^{-1}. All DFT calculations were spin polarized, and both ferromagnetic and antiferromagnetic configurations were considered in systems with unpaired electrons. For binary oxides, antiferromagnetic spin orderings were systematically enumerated using the methods implemented in ENUMLIB [69–72] as made available in PYMATGEN. For ternary oxides, only manually chosen spin orderings were considered owing to the large number of configurational degrees of freedom. For the O–O binding energy analysis of Fig. 2, DFT calculations with the GGA functional by PBE [11] were performed using parameters identical to those of the SCAN+rVV10 calculations.

The DFT + U calculations were performed in the rotationally invariant approximation [16] applied to the TM d bands as implemented in VASP with PAW. It has previously been established that DFT + U reaction energies change, in good approximation, linearly with the U value over the relevant range [14,39]. The DFT + U energies of binary oxides were estimated by linear interpolation by Wang *et al.* [14] for PBE + U and by Gautam *et al.* [39] and Long *et al.* [44] for SCAN + U parameterization. We use this approach here and generalize it to ternary oxides, i.e., we determine the planes that approximate best the SCAN + U energies of ternary oxides as function of the U values of two TM species. We use at least three different U values per TM species and compound.

III. RESULTS

A. Correction for systematic oxygen energy error

Figure 2 shows the formation energies of binary and ternary oxides as predicted by DFT calculations compared to the experimental reference values. The details of our DFT calculations are given in Sec. II F. As previously reported [14], the PBE functional systematically underestimates the magnitude of the formation energies owing to the O–O overbinding error in O_2 as demonstrated by the offset in the correlation plot [Fig. 2(a)]. In contrast, the correlation plot for the SCAN functional [Fig. 2(b)] does not exhibit any offset indicating no systematic error. Thus, no oxygen energy correction is required for the SCAN functional, and $\varepsilon_{O_2}^{\text{corr}} = 0$ eV, as also found previously in Refs. [39,43,44].

B. Impact of regularization

To determine a suitable value for the regularization parameter λ of Eq. (13), we performed a Hubbard-U value optimization as described above with values of λ varying from 0.00 to 0.05. Figure S2 shows how the RMSE of the predicted reaction energies, the U values, and the DFT/DFT + U compatibility correction change with the regularization parameter. As λ increases from 0.00 to 0.01, the increase

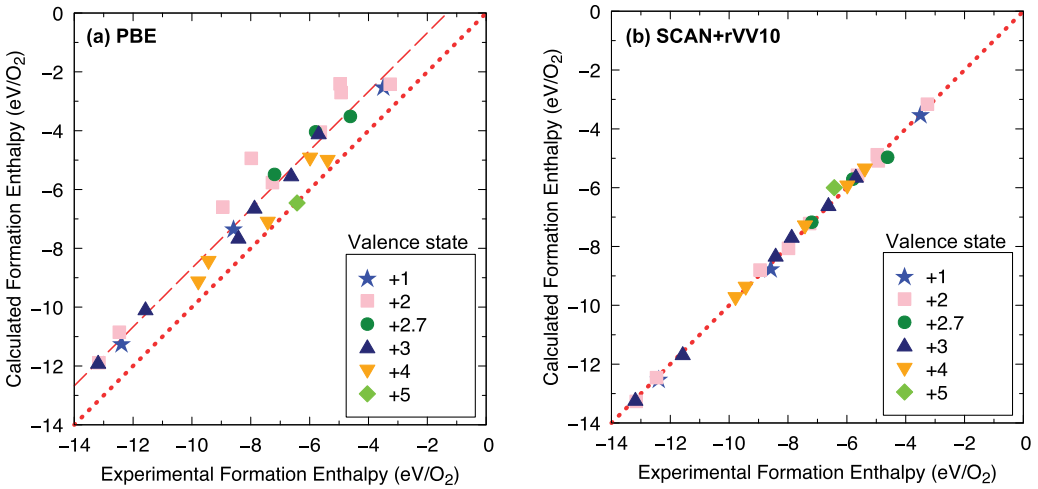

FIG. 2. Comparison of (a) PBE and (b) SCAN+rVV10 formation enthalpies with experimental reference values. In contrast to PBE, SCAN+rVV10 formation enthalpies do not show any systematic shift due to oxygen overbinding. No empirical oxygen energy correction is needed for SCAN+rVV10. As noted in Sec. II B, a sample of additional main-group oxides are included. See Supplemental Material Table S3.

of the RMSE is negligible, but the U values of some of the TM species are already significantly lowered. Specifically, the change of the U values of Ti, Cr, and Co decrease by ∼0.5 eV. Increasing the L2 regularization parameter further results in a notable increase of the RMSE for values of λ beyond 0.01 eV (see Fig. S2). Therefore, we chose $\lambda = 0.01$ for the analysis in the remainder of this work.

C. Reaction similarity

We performed a PCA of the 1,710 reactions in our reference data set in an initial vector representation with 57 dimensions, as described above. As shown in Figs. S3, 25 principal components (PCs) can explain >95% of the variance of the data set. Reactions that share reactants and/or products have similar PC representations, whereas the reaction type (e.g., formation reactions vs. oxide reactions) does not strongly correlate with the PCs, as seen for the example of the first two PCs in Fig. S4.

To group reactions by similarity in the PC representation, we next performed a k-means cluster analysis. The k-means clustering method requires that the number of clusters (i.e., *reaction groups* here) be defined beforehand. Figure S5 shows how the optimal U value, the value of the DFT/DFT + U (Jain) correction, and the RMSE of the reaction energies vary with the number of clusters, which were chosen as multiples of the number of oxides in our reference data set (37, 74, 111, 148, 222, 444, 666, 888, 1110, 1332, 1554, and 1700). The impact of grouping the reactions on the optimal U value emerges as the number of clusters is reduced from 1700. As seen in the figure, the optimal U value is minimally affected by the number of clusters down to about 444, with the exception of Cr where it decreases from ∼4 to ∼3 eV. Not surprisingly, when smaller numbers of clusters are employed, 222 and below, the optimal U values for several elements show more significant variations. Overall, at intermediate numbers of clusters, there is a broad plateau in the optimal U values. Based on this analysis, we chose 888 clusters (=24 × 37), and all reactions were weighted according to the size of their reaction group in the U-value optimizations reported in the following.

D. Hubbard-U values for different fitting strategies

We performed U-value optimizations using the two strategies detailed under the theoretical framework in the previous section, i.e., with and without DFT/DFT + U compatibility (Jain) corrections. In both cases, the iterative least-squares fit was first performed without regularization and then with L2 regularization (with $\lambda = 0.01$) as described above. No oxygen energy correction was introduced.

The obtained U values are given in Table I. Significant differences of more than 1 eV are seen between U values optimized with and without Jain corrections. Without Jain corrections, the U values for Ti, Cr, Mn, Fe, and Co are smaller, while that for Ni increases. By design, L2 regularization leads to smaller U values. Without Jain correction, the differences due to the L2 regularization are generally small and range from <0.1 to ∼0.3 eV. When Jain correction energies are used, L2 regularization has a more notable impact, and the U values for Cr and Co decrease from 5.01 to 2.86 eV and from 2.84 to 2.08 eV, respectively. In general, the U values optimized for SCAN are already of modest scale.

E. DFT/DFT + U compatibility (Jain) corrections

Table I also lists the DFT/DFT + U compatibility (Jain) corrections of the different TM species corresponding to the U values determined with strategy (2). As seen in the table, the Jain correction energies obtained from L2-regularized optimization are generally smaller than those obtained without regularization. The Jain corrections are largest in absolute value for those TM species for which the U values vary most among the different optimization strategies (Ti, Cr, Mn, Fe, and Co). The sign of the corrections is positive with the exception of a small negative correction for Ni (−0.15 eV).

TABLE I. U values and Jain DFT/DFT + U compatibility corrections obtained for different optimization strategies with and without L2 regularization. All U values and SCAN/SCAN + U corrections are given in electronvolts (eV). The recommended values are shown in bold.

	Ti	V	Cr	Mn	Fe	Co	Ni	Cu
Optimized U values without SCAN/SCAN + U correction								
U value	0.60	0.95	1.09	1.49	0.91	1.51	0.59	0.00
L2-regularized optimized U values without SCAN/SCAN + U correction								
U value	0.54	0.93	1.02	1.42	0.86	1.24	0.38	0.00
Optimized U values with SCAN/SCAN + U correction after Jain *et al.*								
U value	2.54	0.95	5.01	2.23	2.01	2.84	0.42	0.00
Jain correction	1.30	0.05	2.23	0.68	0.82	0.74	−0.15	0.02
L2-regularized optimized U values with SCAN/SCAN + U correction after Jain *et al.*								
U value	**1.87**	**0.93**	**2.86**	**1.99**	**1.88**	**2.08**	**0.41**	**0.00**
Jain correction	**0.89**	**0.04**	**1.01**	**0.58**	**0.74**	**0.50**	**−0.15**	**0.02**

F. Validation and accuracy estimate of the different parametrizations

Figure 3 shows the RMSEs of oxide formation energies and oxide reaction energies relative to the experimental reference data as obtained from LOOCV. See also Supplemental Material Table S4 for a list of the cross-validation errors.

As expected, the overall RMSE decreases as Hubbard-U and Jain corrections are introduced. However, the error does not decrease equally for all classes of reactions. The accuracy of the binary oxide reactions not involving O_2 does not improve when a Hubbard-U correction is introduced, and only a small improvement is seen for ternary oxide reactions that involve O_2. Significant improvement is seen for both binary and ternary oxide formation energies and for the energies of binary oxide reactions involving O_2. The error decreases from 0.17 to 0.10 eV/atom and from 0.12 eV/atom to 0.03 eV/atom for binary and ternary formation energies, respectively. The error of the reaction energies of binary oxides involving O_2 improves from 0.14 to 0.07 eV/atom. Interestingly, the Hubbard-U correction as well as the additional DFT/DFT + U compatibility correction after Jain both contribute to reducing the error in these cases. However, a significant impact can be realized without the Jain correction.

The good predictive power of SCAN + U with the U+ Jain + L2 parametrization for formation energies can also be seen in Fig. 4, in which the computed formation energies are

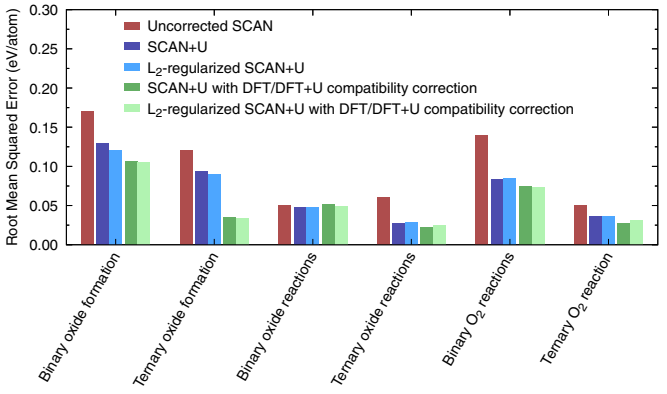

FIG. 3. RMSEs for oxide formation and oxide reaction energies predicted by SCAN + U calculations using the four different sets of U values and Jain corrections of Table I. Oxide reactions not involving elemental oxygen as a reactant are labeled *oxide reactions*, whereas those reactions that do involve oxygen are labeled O_2 *reactions*. All SCAN + U error estimates were obtained from leave-one-out cross validation.

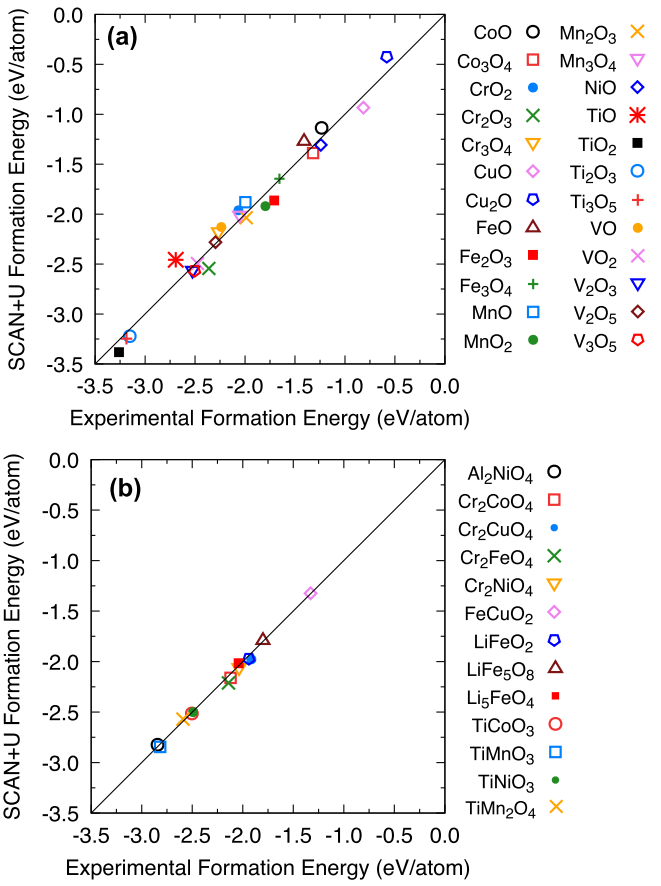

FIG. 4. Comparison of predicted enthalpies of formation ($\Delta_f H^\circ$) from SCAN + U with experimental reference values (298K) for (a) binary and (b) ternary transition-metal oxides. SCAN + U predictions are based on the L2-regularized optimized U values and DFT/DFT + U compatibility corrections of Table I. All data points shown were evaluated with leave-one-out cross validation. Each point represents a true prediction based on the U values fit to the rest of the data set.

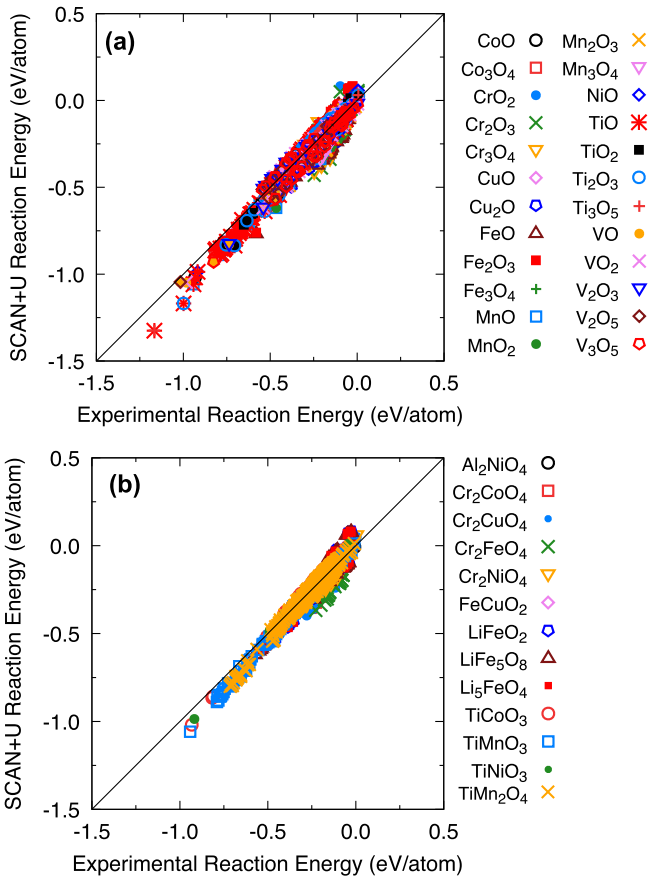

FIG. 5. Comparison of oxide reaction energies, both with and without O_2 as a reactant, predicted by SCAN + U (L2-regularized U values and Jain correction) with their reference values derived from experimental formation enthalpies for (a) binary oxides and (b) ternary oxides. Each oxide occurs in multiple reactions, so that the same symbol appears multiple times in the graphs. All data points represent true predictions from leave-one-out cross validation.

compared with their experimental references. As seen in the figure, the LOOCV predictions are centered around the optimal diagonal for binary oxides [Fig. 4(a)] and ternary oxides [Fig. 4(b)], respectively. The most noticeable remaining error, with a magnitude of ∼0.2 eV, is seen for the binary oxide TiO.

An equivalent analysis of the oxide reaction energies is shown in Fig. 5. Note that the reaction energies vary less than the formation energies, and therefore the energy scale in Fig. 5 is smaller than that of Fig. 4, so the scattering appears more significant. If an oxide appears in multiple reactions, its corresponding symbol appears multiple times in the graphs. Multiple compounds (reactants and products) participate in each oxide reaction, and the data points of all oxides involved in the same reaction are shown with overlapping symbols in Fig. 5.

The largest errors are again seen for reactions involving TiO, in agreement with the error analysis of the formation energies. Note that all data points shown in Fig. 5 are true predictions obtained from LOOCV. This means, for each oxide compound in our database, a U parametrization was fitted on a data set that did not include any reactions involving this specific oxide compound. The resulting parametrization was used to predict all of the derived reaction energies. Symbols and colors in Fig. 5 indicate reaction energies that were evaluated together with the same U-value parametrization.

As a final test of the optimized SCAN + U parameterization, we consider the phase diagram of the binary oxides that can be obtained by constructing the lower convex hull of the formation energies [5]. Only compounds that lie on the convex hull are thermodynamically stable, and the shape of the hull determines the chemical potential stability range of each phase. In Fig. 6, the formation energy convex hulls of Mn and Co oxides as predicted by SCAN and SCAN + U are compared with the experimental reference, and the corresponding constructions for Ti, V, Cr, and Fe are shown in supporting Fig. S6. The differences between SCAN and SCAN + U are most pronounced for Mn and Co with the result that SCAN + U predicts the shape of the convex hulls in better agreement with experiment than uncorrected SCAN. Unlike uncorrected SCAN, SCAN + U also correctly predicts both Co oxides to be stable. As seen in Fig. S6, the differences between SCAN and SCAN + U are smaller for the other transition metal species. For Ti and Fe, both SCAN and SCAN + U predict the shape of the hull in good agreement with experiment but incorrectly predict some of the oxides to be slightly unstable. Both methods correctly predict all V oxides to be stable, though the + U correction improves the shape of the hull. For Cr oxides, SCAN predicts two and SCAN + U predicts only one of its three oxides to be stable.

IV. DISCUSSION

The present study considers the Hubbard-U values and DFT/DFT + U compatibility corrections in a unified optimization approach across the class of 3d transition metal oxides. By design, the data set includes ternary oxides for which experimental formation energies are available. This results in an interconnected dataset, linking the determination of the parameters across the 3d series, that supports a systematic cross-validation analysis of the errors.

We find that the SCAN functional does not exhibit any systematic error in the O_2 binding energy, and an empirical oxygen correction is therefore not needed. This result is in agreement with a previous study by Isaacs and Wolverton [38], who found no systematic over- or underbinding in formation energies predicted by the SCAN functional (without Hubbard-U correction).

A Hubbard-U correction further reduces the error of predicted binary formation energies by more than 40% from 0.17 to 0.10 eV/atom if a DFT/DFT + U compatibility (Jain) correction is introduced as well. The error in ternary formation energies is reduced by 75% from 0.12 to 0.03 eV/atom. Without the Jain correction, that is, only through adjustment of U value, the expected errors of predicted binary and ternary formation energies are 0.12 eV/atom and 0.09 eV/atom, respectively. This is still an improvement of ∼30% and 25% compared to uncorrected SCAN. Note that a Hubbard-U parametrization without additional Jain correction has the advantage that it can be used with standard DFT codes without the need of additional postprocessing of the predicted DFT + U energies.

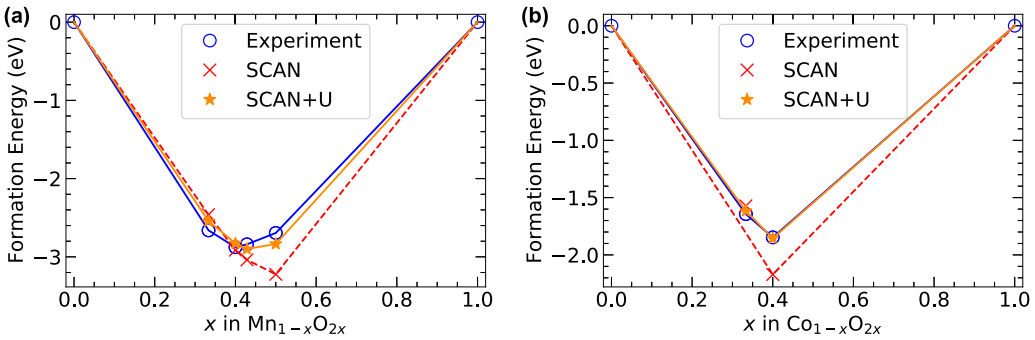

FIG. 6. Formation energies and convex-hull constructions of the binary oxides of (a) Mn and (b) Co. Equivalent visualizations for Ti, V, Cr, and Fe are shown in supporting Fig. S6. Formation energies computed with uncorrected SCAN+rVV10 (red crosses) and with inclusion of L_2-regularized optimized Hubbard-U values and DFT/DFT + U corrections (orange stars) are compared to experimental reference values (blue circles).

We note that the experimental reference data used as target for the U-value optimization is also subject to uncertainties. By comparing the formation enthalpies from various sources for a large number of compounds this uncertainty was previously estimated to be ∼0.08 eV/atom [52]. For the present work, we found the formation enthalpies of the CRC Handbook of Chemistry and Physics [53] to be generally within ∼0.02 eV/atom of the NIST-JANAF database [73]. Hence, a residual optimization error of at least this magnitude has to be expected.

Figure 7 shows the distributions of U values and Jain corrections for each TM species obtained with the LOOCV method when L2 regularization is employed. In the LOOCV procedure, the optimization is independently carried out while leaving out data deriving from one of the 37 compounds. The scatter among the 37 U values and Jain corrections indicates sensitivity to data inclusion. For comparison, the values derived from a single optimization over the full dataset are also shown for each TM species. As seen in the figure, the scatter in the values is low. For all TM species, most of the optimized U values lie within a range of ±0.5 eV from an average value. The values are also well centered on the single optimization results.

Note that without grouping of similar reactions and without L2 regularization, the scattering is significantly larger, leading to greater uncertainty in the U values (Fig. S7). Table S5 lists the standard deviation of the U values and Jain corrections for different optimization strategies as a measure of the scattering. The combination of reaction grouping and L2 regularization reduces the standard deviation of the U values for all TM species except Fe and significantly reduces the uncertainty of the parameters for Ti and Cr. As seen in the table, the reduction is mostly due to the reaction grouping. The same trend is observed for the Jain correction values. Furthermore, although the impact of L2 regularization on the U values is significant (maximum impact 2.2 eV for Cr), regularization does not noticeably affect the model accuracy, as seen in Fig. 3. Finally, regularization results in U values that are systematically smaller (Table I). As a general rule, DFT + U calculations are technically easier to execute, particularly to reliably converge to the correct electronic ground state, for smaller U values [31]. Overall, this suggests that our use of L2 regularization has led to an improved set of Hubbard-U values and DFT/DFT + U compatibility corrections for application with SCAN to thermochemical properties of 3d TM oxide compounds.

The resulting parameters for SCAN + U (with Jain correction and L2 regularization) lead to reaction energies that reproduce experiment rather accurately with an error of less than 0.08 eV RMSE across the dataset. This is comparable to the estimated errors in the underlying experimental dataset. The parameters found here also yield overall improved phase

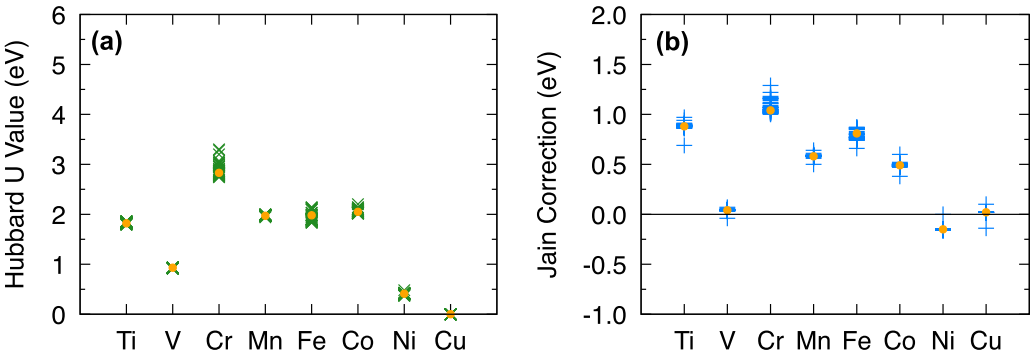

FIG. 7. Distribution of (a) U values and (b) Jain correction values determined from the full set of leave-one-our cross-validation optimizations with L2 regularization (U+ Jain + L2 parametrization). The values obtained from a single optimization on the entire data set are indicated by orange points.

diagrams for binary oxides. However, the RMSE for a few formation and reaction energies exceeds 0.2 eV. Reactions involving titanium (II) exhibit the largest errors, and both uncorrected SCAN and SCAN + U incorrectly predict TiO to be unstable (Figure S6). This may indicate that no single U value is simultaneously appropriate for both Ti^{2+} (TiO), Ti^{3+} (Ti_2O_3), and Ti^{4+} (TiO_2 and the ternary oxides). To a smaller degree, the same effect is seen for Fe and Mn, which also form oxides with multiple different valence states. As seen in Fig. 4, Fe_3O_4 (Fe^{2+} and Fe^{3+}) falls on the ideal diagonal while FeO (Fe^{2+}) and Fe_2O_3 (Fe^{3+}) are slightly over- and underbound, respectively. Similarly, the formation enthalpy of the Mn oxide Mn_2O_3 (Mn^{3+}) is most accurately reproduced, whereas MnO (Mn^{2+}) and MnO_2 (Mn^{4+}) deviate in opposite directions. However, for both Fe and Mn oxides, the optimal U value is an excellent compromise for all oxides and significantly improves the accuracy of reaction energies. For binary Mn oxides, SCAN + U also leads to an improved phase diagram that is in excellent agreement with experiment (Fig. 6). Without + U correction, SCAN incorrectly predicts two of the Fe oxides to be unstable. The + U correction does not correct this error but results in an overall quantitative improvement of the relative energies of the iron oxides (Fig. S6). SCAN + U also improves the relative energies of the Cr oxides, however, only one out of three oxides is predicted to be stable. Based on this observation, SCAN + U would not be able to reproduce the phase diagram of Cr oxides correctly, irrespective of the U value. However, the absolute value of reaction and formation energies of Cr oxides as predicted by the optimized (average) U value are nevertheless in reasonable agreement with experiment ($\sim \pm 0.2$ eV).

As noted in the introduction, the U value is, in principle, dependent on the oxidation state (d-band occupancy) and on the electronic screening of the local Coulomb interactions in different compounds and structures [20]. It is an approximation to assume a constant value for each TM species across all oxides. But in practical applications, the approximation of a single U value is essential. While a correction based on an average U value may not always achieve a correction of qualitative flaws in phase diagrams, such as missing phases, we find that it generally leads to a quantitative improvement of the formation energy convex hull.

Recently, Long, Gautam, and Carter reported a SCAN + U parameterization for the calculation of reaction energies of 3d TM oxides [39,44], not including formation reactions from the elemental metals. For some of the TM species, our U values, which were optimized for general oxide reactions including formation reactions, differ significantly from these previous reports. Our U values for Fe (1.9 eV) and Ni (0.4 eV) are both significantly smaller than the values reported by Long *et al.* (Fe: 3.1 eV, Ni: 2.5 eV). Our optimization yields a significant U value for Cr (2.9 eV) whereas Long *et al.* found a U value of 0 eV (i.e., no Hubbard-U correction) to be optimal for oxide reactions. These differences further exemplify the importance of selecting U values for the intended application, an inherent limitation of DFT + U. Both our approach and the approach by Long *et al.* yield a U value of zero for Cu.

We note that Long *et al.* discuss that a U value of 0 eV for Cr is counter-intuitive and appears to be an anomaly, as one might expect a nonzero optimal U value for Cr that is similar in magnitude to the values for V and Mn. Long *et al.* attributed this behavior to error cancellation caused by potential inaccuracies in the experimental formation enthalpy of metastable CrO and the metallic character of CrO_2 [44]. Our data set does not contain the metastable CrO. We did include CrO_2, as well as Cr_2O_3 and Cr_3O_4 and the stable, ternary Cr(III) spinels (Cr_2CoO_4, Cr_2FeO_4, and Cr_2NiO_4). Hence, the difference in U value might also be due to the different choice of experimental reference.

Even though the U-value optimization determined that $U = 0$ eV is optimal for Cu, a small Jain correction of 0.02 eV is found to improve the overall accuracy of SCAN for Cu oxides. Hence, the correction energy is not only accounting for DFT/DFT + U compatibility but also compensates other systematic errors in the formation energies. The Jain correction is only applied to oxides and only affects the formation energies. Note that alternatively an energy shift with opposite sign could be applied to the energy of the base metal to achieve an equivalent correction. Such an energy adjustment of the elements was developed in the fitted elemental-phase reference energies (FERE) by Stevanović and coworkers [18], as an empirical correction to improve formation enthalpy predictions. In the FERE approach, the elemental reference energies were determined using a least-squares fit for a set of fixed U values, which achieves a formation-energy accuracy for ternary oxides that is similar to our approach [18]. The authors did not report a benchmark for reaction energies.

We note that the absolute value of the optimized U values reported here are specific for the commonly used rotationally averaged Hubbard-U methodology by Dudarev *et al.* [16] The values can, to some extent, also depend on the basis set and implementation, and therefore transferability should be tested when DFT + U implementations other than PAW as implemented in VASP are used. However, we expect the reported trends, such as relative U-value magnitudes, to be more general. The optimization methodology itself is also general and not limited to any specific basis set or implementation.

Finally, we note that while the focus of the present work is on the prediction of formation energies and other oxide reaction energies with the SCAN functional, the optimization framework for the iterative U value and Jain correction fit is general and could also be used to optimize U values for other DFT functionals and for other targets, for example, to reproduce band gaps or lattice parameters.

V. SUMMARY AND CONCLUSIONS

Empirically corrected DFT calculations can yield quantitative predictions of TM oxide properties, but determining reliable and transferable parameters for DFT + U methods remains a significant challenge. In this article, the parameterization of three common empirical corrections to DFT (oxygen overbinding, Hubbard-U, and DFT/DFT + U compatibility correction) was expressed as a unified optimization problem that can be solved with the method of least squares. As an example of practical relevance, we chose to target thermochemistry of the oxides of the 3d TM species (Ti, V, Cr, Mn, Fe, Co, Ni, Cu). To that purpose, we assembled a substantial database of experimental formation energies (37 compounds in total) from the literature for fitting and

validation. In addition to the formation reactions, we also considered all unique reactions involving these oxides with each other and with oxygen gas, for a total of 1710 derived reaction energies. To avoid biases in the data set, we developed a methodology for the grouping of similar reactions based on principal component analysis and k-means clustering. This interconnected and substantial database enabled systematic statistical evaluation of the accuracy of the derived parameters using a cross-validation methodology. In distinction over the typical procedure that focuses on one TM species at a time, this approach yields parameters for a family of elements with a procedure that is easily automated. Applied to the SCAN + U density functional, we find that the error in predicted binary (ternary) oxide formation energies is reduced by ∼40% (75%) if all three correction terms are included, as determined by leave-one-out cross validation. Without a SCAN/SCAN + U compatibility correction (which requires postprocessing of DFT calculations with common DFT software), the improvement compared to uncorrected SCAN calculations is still ∼30% (25%).

The proposed framework, which incorporates robust statistical methods, offers an approach for the simultaneous optimization of U values for oxide and formation reactions. It minimizes arbitrariness in determining the empirical parameters for DFT + U methods while providing an error estimate for the parameter values and the predicted reaction energies. The reported SCAN/SCAN + U parameterization specifically enables accurate predictions of 3d TM metal and oxide reactions. Moreover, our framework, which has been made available as free and open-source software, is not limited to the SCAN functional or to the target of reaction energetics. It can be applied to the correction of any density functional in the context of DFT + U methods.

The formation and reaction energy data and software implementation of our approach are publicly available (see Ref. [74]).

ACKNOWLEDGMENTS

This research was carried out in part at the Center for Functional Nanomaterials, which is a U.S. Department of Energy (DOE) Office of Science Facility, and used resources at the Scientific Data and Computing Center of the Computational Science Initiative, at Brookhaven National Laboratory under Contract No. DE-SC0012704. DFT calculations and machine-learning model construction also made use of the Extreme Science and Engineering Discovery Environment (XSEDE), which is supported by National Science Foundation Grant No. ACI-1053575 (allocation No. DMR14005). J.A.G.T. and A.U. acknowledge support by the National Science Foundation (NSF) under Grant No. DMR-1940290.

N.A. and M.S.H. conceived the project. N.A. implemented the methodology. N.A. and J.A.G.T. performed the DFT calculations. N.A. performed the parameter optimization. N.A. and A.U. analyzed the data. N.A., A.U., and M.S.H. wrote the manuscript, which was revised by all authors.

The authors declare no competing interests.

[1] P. Hohenberg and W. Kohn, Inhomogeneous electron gas, Phys. Rev. **136**, B864 (1964).

[2] W. Kohn and L. J. Sham, Self-consistent equations including exchange and correlation effects, Phys. Rev. **140**, A1133 (1965).

[3] A. J. Medford, A. Vojvodic, J. S. Hummelshøj, J. Voss, F. Abild-Pedersen, F. Studt, T. Bligaard, A. Nilsson, and J. K. Nørskov, From the sabatier principle to a predictive theory of transition-metal heterogeneous catalysis, J. Catal. **328**, 36 (2015).

[4] A. Jain, Y. Shin, and K. A. Persson, Computational predictions of energy materials using density functional theory, Nat. Rev. Mater. **1**, 1 (2016).

[5] A. Urban, D.-H. Seo, and G. Ceder, Computational understanding of li-ion batteries, Npj Comput. Mater. **2**, 16002 (2016).

[6] Z. W. Seh, J. Kibsgaard, C. F. Dickens, I. Chorkendorff, J. K. Nørskov, and T. F. Jaramillo, Combining theory and experiment in electrocatalysis: Insights into materials design, Science **355**, eaad4998 (2017).

[7] J. P. Perdew and W. Yue, Accurate and simple density functional for the electronic exchange energy: Generalized gradient approximation, Phys. Rev. B **33**, 8800 (1986).

[8] A. J. Cohen, P. Mori-Sánchez, and W. Yang, Insights into current limitations of density functional theory, Science **321**, 792 (2008).

[9] J. P. Perdew and A. Zunger, Self-interaction correction to density-functional approximations for many-electron systems, Phys. Rev. B **23**, 5048 (1981).

[10] Y. Zhang and W. Yang, A challenge for density functionals: Self-interaction error increases for systems with a noninteger number of electrons, J. Chem. Phys. **109**, 2604 (1998).

[11] J. P. Perdew, K. Burke, and M. Ernzerhof, Generalized Gradient Approximation Made Simple, Phys. Rev. Lett. **77**, 3865 (1996).

[12] S. Kurth, J. P. Perdew, and P. Blaha, Molecular and solid-state tests of density functional approximations: LSD, GGAs, and Meta-GGAs, Int. J. Quantum Chem. **75**, 889 (1999).

[13] D. C. Patton, D. V. Porezag, and M. R. Pederson, Simplified generalized-gradient approximation and anharmonicity: Benchmark calculations on molecules, Phys. Rev. B **55**, 7454 (1997).

[14] L. Wang, T. Maxisch, and G. Ceder, Oxidation energies of transition metal oxides within the GGA+U framework, Phys. Rev. B **73**, 195107 (2006).

[15] V. I. Anisimov, J. Zaanen, and O. K. Andersen, Band theory and Mott insulators: Hubbard u instead of stoner I, Phys. Rev. B **44**, 943 (1991).

[16] S. L. Dudarev, G. A. Botton, S. Y. Savrasov, C. J. Humphreys, and A. P. Sutton, Electron-energy-loss spectra and the structural stability of nickel oxide: An LSDA+U study, Phys. Rev. B **57**, 1505 (1998).

[17] S. Lany, Semiconductor thermochemistry in density functional calculations, Phys. Rev. B **78**, 245207 (2008).

[18] V. Stevanović, S. Lany, X. Zhang, and A. Zunger, Correcting density functional theory for accurate predictions of compound enthalpies of formation: Fitted elemental-phase reference energies, Phys. Rev. B **85**, 115104 (2012).

[19] R. Friedrich, D. Usanmaz, C. Oses, A. Supka, M. Fornari, M. Buongiorno Nardelli, C. Toher, and S. Curtarolo, Coordination corrected *ab initio* formation enthalpies, Npj Comput. Mater. **5**, 1 (2019).

[20] M. Cococcioni and S. de Gironcoli, Linear response approach to the calculation of the effective interaction parameters in the LDA+U method, Phys. Rev. B **71**, 035105 (2005).

[21] B. Himmetoglu, A. Floris, S. de Gironcoli, and M. Cococcioni, Hubbard-corrected DFT energy functionals: The LDA+U description of correlated systems, Int. J. Quantum Chem. **114**, 14 (2014).

[22] I. Timrov, N. Marzari, and M. Cococcioni, Hubbard parameters from density-functional perturbation theory, Phys. Rev. B **98**, 085127 (2018).

[23] S. Lutfalla, V. Shapovalov, and A. T. Bell, Calibration of the DFT/GGA+U method for determination of reduction energies for transition and rare earth metal oxides of Ti, V, Mo, and Ce, J. Chem. Theory Comput. **7**, 2218 (2011).

[24] A. Jain, G. Hautier, S. P. Ong, C. J. Moore, C. C. Fischer, K. A. Persson, and G. Ceder, Formation enthalpies by mixing GGA and GGA+U calculations, Phys. Rev. B **84**, 045115 (2011).

[25] G. Hautier, S. P. Ong, A. Jain, C. J. Moore, and G. Ceder, Accuracy of density functional theory in predicting formation energies of ternary oxides from binary oxides and its implication on phase stability, Phys. Rev. B **85**, 155208 (2012).

[26] A. Jain, S. P. Ong, G. Hautier, W. Chen, W. D. Richards, S. Dacek, S. Cholia, D. Gunter, D. Skinner, G. Ceder, and K. A. Persson, Commentary: The materials project: A materials genome approach to accelerating materials innovation, APL Mater. **1**, 011002 (2013).

[27] D.-H. Seo, A. Urban, and G. Ceder, Calibrating transition-metal energy levels and oxygen bands in first-principles calculations: Accurate prediction of redox potentials and charge transfer in lithium transition-metal oxides, Phys. Rev. B **92**, 115118 (2015).

[28] F. Zhou, M. Cococcioni, C. A. Marianetti, D. Morgan, and G. Ceder, First-principles prediction of redox potentials in transition-metal compounds with LDA+U, Phys. Rev. B **70**, 235121 (2004).

[29] H. Park, A. J. Millis, and C. A. Marianetti, Computing total energies in complex materials using charge self-consistent DFT + DMFT, Phys. Rev. B **90**, 235103 (2014).

[30] A. Paul and T. Birol, Applications of DFT + DMFT in materials science, Annu. Rev. Mater. Res. **49**, 31 (2019).

[31] B. Meredig, A. Thompson, H. A. Hansen, C. Wolverton, and A. van de Walle, Method for locating low-energy solutions within DFT+U, Phys. Rev. B **82**, 195128 (2010).

[32] J. W. Bennett, I. Grinberg, P. K. Davies, and A. M. Rappe, Pb-free semiconductor ferroelectrics: A theoretical study of Pd-substituted $BaTi_{1-x}Ce_xO_3$ solid solutions, Phys. Rev. B **82**, 184106 (2010).

[33] J. M. Garcia-Lastra, J. S. G. Myrdal, R. Christensen, K. S. Thygesen, and T. Vegge, DFT+U study of polaronic conduction in Li_2O_2 and Li_2CO_3: Implications for Li–air batteries, J. Phys. Chem. C **117**, 5568 (2013).

[34] J. B. Varley, V. Viswanathan, J. K. Nørskov, and A. C. Luntz, Lithium and oxygen vacancies and their role in Li_2O_2 charge transport in Li_2O_2 Batteries, Energy Environ. Sci. **7**, 720 (2014).

[35] J. Sun, A. Ruzsinszky, and J. P. Perdew, Strongly Constrained and Appropriately Normed Semilocal Density Functional, Phys. Rev. Lett. **115**, 036402 (2015).

[36] H. Peng, Z.-H. Yang, J. P. Perdew, and J. Sun, Versatile van Der Waals Density Functional Based on a Meta-Generalized Gradient Approximation, Phys. Rev. X **6**, 041005 (2016).

[37] A. Chakraborty, M. Dixit, D. Aurbach, and D. T. Major, Predicting accurate cathode properties of layered oxide materials using the SCAN Meta-GGA density functional, Npj Comput. Mater. **4**, 1 (2018).

[38] E. B. Isaacs and C. Wolverton, Performance of the strongly constrained and appropriately normed density functional for solid-state materials, Phys. Rev. Mater. **2**, 063801 (2018).

[39] G. Sai Gautam and E. A. Carter, Evaluating transition metal oxides within DFT-SCAN and SCAN+U frameworks for solar thermochemical applications, Phys. Rev. Mater. **2**, 095401 (2018).

[40] C. J. Bartel, A. W. Weimer, S. Lany, C. B. Musgrave, and A. M. Holder, The role of decomposition reactions in assessing first-principles predictions of solid stability, Npj Comput. Mater. **5**, 1 (2019).

[41] J. H. Yang, D. A. Kitchaev, and G. Ceder, Rationalizing accurate structure prediction in the meta-GGA SCAN functional, Phys. Rev. B **100**, 035132 (2019).

[42] A. M. Cooper, J. Kästner, A. Urban, and N. Artrith, Efficient training of ANN potentials by including atomic forces via taylor expansion and application to water and a transition-metal oxide, Npj Comput. Mater. **6**, 1 (2020).

[43] E. B. Isaacs, S. Patel, and C. Wolverton, Prediction of Li intercalation voltages in rechargeable battery cathode materials: effects of exchange-correlation functional, van Der Waals interactions, and Hubbard U, Phys. Rev. Mater. **4**, 065405 (2020).

[44] O. Y. Long, G. Sai Gautam, and E. A. Carter, Evaluating optimal U for $3d$ transition-metal oxides within the SCAN+U framework, Phys. Rev. Mater. **4**, 045401 (2020).

[45] S. Kim, Lattice and electronic properties of VO_2 with the SCAN($+U$) approach, J. Korean Phys. Soc. **78**, 613 (2021).

[46] N. E. Kirchner-Hall, W. Zhao, Y. Xiong, I. Timrov, and I. Dabo, Extensive Benchmarking of DFT+U Calculations for Predicting Band Gaps, Appl. Sci. **11**, 2395 (2021).

[47] J. Kaczkowski, M. Pugaczowa-Michalska, and I. Płowaś-Korus, Comparative density functional studies of pristine and doped bismuth ferrite polymorphs by GGA + U and Meta-GGA SCAN + U, Phys. Chem. Chem. Phys. **23**, 8571 (2021).

[48] D. Mutter, D. F. Urban, and C. Elsässer, Determination of formation energies and phase diagrams of transition metal oxides with DFT + U, Materials **13**, 4303 (2020).

[49] E. T. Turkdogan, *Physical Chemistry of High Temperature Technology* (Academic Press, New York, 1980).

[50] O. Kubaschewski, C. B. Alcock, P. J. Spencer, and O. Kubaschewski, *Materials Thermochemistry, 6th ed.* (Pergamon Press, New York, 1993).

[51] J. E. Saal, S. Kirklin, M. Aykol, B. Meredig, and C. Wolverton, Materials design and discovery with high-throughput density functional theory: The open quantum materials database (OQMD), JOM **65**, 1501 (2013).

[52] S. Kirklin, J. E. Saal, B. Meredig, A. Thompson, J. W. Doak, M. Aykol, S. Rühl, and C. Wolverton, The open quantum materials database (OQMD): Assessing the accuracy of DFT formation energies, Npj Comput. Mater. **1**, 1 (2015).

[53] J. R. Rumble, T. J. Bruno, and M. J. Doa, *CRC Handbook of Chemistry and Physics a Ready-Reference Book of Chemical and Physical Data* (CRC Press, Boca Raton, FL, 2020).

[54] See Supplemental Material at http://link.aps.org/supplemental/10.1103/PhysRevMaterials.6.035003 for Supplemental tables with formation enthalpies, the RMSE values of Fig. 3, standard deviations of the U values, and list of the considered oxide reactions. Supplemental figures with a flowchart, additional convergence analyses, additional convex-hull plots, and the distribution of U values and DFT/DFT+U compatibility corrections.

[55] S. P. Ong, W. D. Richards, A. Jain, G. Hautier, M. Kocher, S. Cholia, D. Gunter, V. L. Chevrier, K. A. Persson, and G. Ceder, Python materials genomics (Pymatgen): A robust, open-source python library for materials analysis, Comput. Mater. Sci. **68**, 314 (2013).

[56] K. Pearson, LIII. On lines and planes of closest fit to systems of points in space, Lond. Edinb. Dubl. Philos. Mag. J. Sci. **2**, 559 (1901).

[57] S. Lloyd, Least squares quantization in PCM, IEEE Trans. Inf. Theory **28**, 129 (1982).

[58] F. Pedregosa, G. Varoquaux, A. Gramfort, V. Michel, B. Thirion, O. Grisel, M. Blondel, P. Prettenhofer, R. Weiss, V. Dubourg, J. Vanderplas, A. Passos, D. Cournapeau, M. Brucher, M. Perrot, and É. Duchesnay, Scikit-learn: Machine learning in python, J. Mach. Learn. Res. **12**, 2825 (2011).

[59] S. Curtarolo, D. Morgan, and G. Ceder, Accuracy of *ab initio* methods in predicting the crystal structures of metals: A review of 80 binary alloys, Calphad **29**, 163 (2005).

[60] A. E. Hoerl and R. W. Kennard, Ridge regression: Biased estimation for nonorthogonal problems, Technometrics **12**, 55 (1970).

[61] A. Celisse, Optimal cross-validation in density estimation with the L^2-loss, Ann. Stat. **42**, 1879 (2014).

[62] N. Artrith, Z. Lin, and J. G. Chen, Predicting the activity and selectivity of bimetallic metal catalysts for ethanol reforming using machine learning, ACS Catal. **10**, 9438 (2020).

[63] P. E. Blöchl, Projector augmented-wave method, Phys. Rev. B **50**, 17953 (1994).

[64] G. Kresse and J. Hafner, *Ab initio* molecular dynamics for liquid metals, Phys. Rev. B **47**, 558 (1993).

[65] G. Kresse and J. Hafner, *Ab initio* molecular-dynamics simulation of the liquid-metal-amorphous-semiconductor transition in germanium, Phys. Rev. B **49**, 14251 (1994).

[66] G. Kresse and J. Furthmüller, Efficiency of *ab initio* total energy calculations for metals and semiconductors using a plane-wave basis set, Comput. Mater. Sci. **6**, 15 (1996).

[67] G. Kresse and J. Furthmüller, Efficient iterative schemes for *ab initio* total-energy calculations using a plane-wave basis set, Phys. Rev. B **54**, 11169 (1996).

[68] R. Sabatini, T. Gorni, and S. de Gironcoli, Nonlocal van Der Waals density functional made simple and efficient, Phys. Rev. B **87**, 041108 (2013).

[69] G. L. W. Hart and R. W. Forcade, Algorithm for generating derivative structures, Phys. Rev. B **77**, 224115 (2008).

[70] G. L. W. Hart and R. W. Forcade, Generating derivative structures from multilattices: Algorithm and application to hcp alloys, Phys. Rev. B **80**, 014120 (2009).

[71] G. L. W. Hart, L. J. Nelson, and R. W. Forcade, Generating derivative structures at a fixed concentration, Comput. Mater. Sci. **59**, 101 (2012).

[72] W. S. Morgan, G. L. W. Hart, and R. W. Forcade, Generating derivative superstructures for systems with high configurational freedom, Comput. Mater. Sci. **136**, 144 (2017).

[73] M. W. Chase, *NIST-JANAF Thermochemical Tables*, 4th ed (American Chemical Society; American Institute of Physics for the National Institute of Standards and Technology, Washington, DC, 1998).

[74] https://github.com/atomisticnet/howru